EDINBURGH INSTRUMENTS

50 YEARS 1971-2021

RMS1000

RAMAN MICROSCOPE

Extending the capabilities to Photoluminescence Microscopy, Time-Resolved Measurements and Fluorescence Lifetime Imaging (FLIM)

- Truly Confocal
- Five-Position Grating Turrets
- Two Spectrograph Options
- Up to Four Simultaneous Detectors

www.edinst.com

Received: 14 May 2020 | Revised: 18 September 2020 | Accepted: 18 September 2020

DOI: 10.1002/jrs.6007

RESEARCH ARTICLE

Journal of RAMAN SPECTROSCOPY WILEY

The impact of ultraviolet laser excitation during Raman spectroscopy of hexagonal boron nitride thin films

Marwa Karim[1,2] | **Joao Marcelo J. Lopes**[1] | **Manfred Ramsteiner**[1]

[1]Paul-Drude-Institut für Festkörperelektronik, Leibniz-Institut im Forschungsverbund Berlin e.V., Berlin, Germany

[2]Physics Department, Faculty of Science, Alexandria University, Alexandria, Egypt

Correspondence
Joao Marcelo J. Lopes, Paul-Drude-Institut für Festkörperelektronik, Leibniz-Institut im Forschungsverbund Berlin e.V., 10117 Berlin, Germany.
Email: lopes@pdi-berlin.de

Funding information
German Egyptian Research Short-Term Programme (GERSS), Grant/Award Number: 57397533; Ministry of Higher Education and Scientific Researches; German Academic Exchange Service

Abstract

We utilized excitation in the ultraviolet (UV) spectral range for the study of hexagonal boron nitride (h-BN) thin films on different substrates by Raman spectroscopy. Whereas UV excitation offers fundamental advantages for the investigation of h-BN and heterostructures with graphene, the actual Raman spectra recorded under ambient conditions reveal a temporal decay of the signal intensity. The disappearance of the Raman signal is found to be induced by thermally activated chemical reactions with ambient molecules at the h-BN surface. The chemical reactions could be strongly suppressed under vacuum conditions which, however, favor the formation of a carbonaceous surface contamination layer. For the improvement of the signal-to-noise ratio under ambient conditions, we propose a line-scan method for the acquisition of UV Raman spectra in atomically thin h-BN, a material which is expected to play a key role in future technologies based on 2D van der Waals heterostructures.

KEYWORDS

2D materials, h-BN, h-BN layer transfer, MBE, UV Raman

1 | INTRODUCTION

Hexagonal boron nitride (h-BN) is a wide band gap semiconductor that is promising for a plethora of applications including neutron detection and quantum information processing.[1,2] It has also been successfully employed as ultra-smooth substrates and encapsulation layers for two-dimensional (2D) materials such as graphene and transition metal dichalcogenides.[3–5] h-BN has a layered crystal structure very similar to that of graphite, with the interaction between the layers being of the weak van der Waals (vdW) type. Within each layer, B and N atoms are connected via sp^2-hybridized bonds forming a hexagonal lattice, which renders this material robustness with excellent chemical and thermal stability.[6,7] Even h-BN crystals with a thickness of a few atomic layers are known to be stable against oxidation up to temperatures around 1000°C.[8] Such excellent properties are complemented by h-BN's efficiency as a dielectric layer. With a dielectric constant that remains almost unaltered from bulk down to a single atomic layer,[9] a high breakdown field of about 9.75 MV/cm has been reported for monolayer-thick h-BN tunneling barriers,[10] which is very promising for the implementation of this material into electronic devices.

The use of thin h-BN crystals with thicknesses that can vary from a single atomic layer to a few tens of nanometers, either as a single material (e.g. hosting single photon sources)[11] or incorporated into hybrid vertical vdW heterostructures,[12] has intensified in the last years. For their preparation, various methods have been employed, the most common still being mechanical

exfoliation of micrometer-sized flakes from bulk h-BN crystals.[12,13] Nevertheless, aiming at the realization of large-area synthesis—a crucial step towards applications—scalable approaches such as chemical vapor deposition (CVD),[14] metalorganic vapor phase epitaxy,[15] atomic layer deposition,[16] and molecular beam epitaxy (MBE)[10,17–21] have been explored as well. Here, it is particularly important to be able to evaluate the quality of the synthesized films regarding their structure and optoelectronic properties and compare it, for instance, with results achieved for state-of-the-art bulk h-BN crystals. Among different characterization methods, Raman spectroscopy has already been employed as a fast and, in principle, nondestructive tool to evaluate the crystalline quality of h-BN. A challenge is, however, that differently from graphene, the characteristic peak of h-BN located between 1360 and 1370 cm^{-1}, which is due to the E_{2g} phonon mode and equivalent to the G peak of graphene,[13,22] has a weak intensity under visible wavelength excitation. The proportionality between its integrated intensity and the number of atomic layers makes Raman analysis of films only a few atomic layers thick especially difficult. Another complication is added when h-BN is combined with graphene in vdW heterostructures: The h-BN E_{2g} phonon mode might interfere with the relatively broad defect-related D peak of graphene appearing in the same spectral regions for visible excitation.[20,21] A similar problem is found for heterostructures formed of h-BN and epitaxial graphene on SiC(0001), where even in the absence of a D peak, the h-BN signal can superimpose with the Raman signal originating from the $6(\sqrt{3} \times \sqrt{3})R30^{\circ}$ interfacial layer between graphene and SiC (also known as buffer layer),[18] which consists of broad bands spreading over 1200 and 1660 cm^{-1}.[23]

In order to overcome all these obstacles, Raman spectroscopy utilizing ultraviolet (UV) excitation has been proposed. Based on calculations and experimental observation, Reich et al. demonstrated that UV excitation (e.g., $\lambda = 244$ nm, or $E_g = 5.08$ eV) during the Raman measurements is more suitable than the visible ones for characterizing h-BN.[24] This is because upon UV laser excitation, the signal due to the E_{2g} optical phonon of h-BN increases, because a certain degree of resonance for the Raman scattering is achieved at an energy of 5.08 eV, which approaches the band gap of the h-BN. Moreover, UV Raman is very useful to analyze h-BN/graphene heterostructures. For the D peak of graphene, a wavenumber shift to 1485 cm^{-1} is expected together with a pronounced quenching of its intensity, when UV excitation with $\lambda = 244$ nm is used.[25] This avoids overlapping between the D peak and the E_{2g} optical phonon of h-BN, which has been proven highly beneficial for the evaluation of the individual properties of h-BN co-existing with graphene in large-area heterostructures.[18,21] Finally, for the case of atomically thin h-BN grown on top of metallic substrates such as Ni, another benefit of Raman analysis under UV excitation is the absence of an inhomogeneous luminescence originating from the underlying metal,[21] which results in a strong background signal and is observed when visible wavelength excitation is employed.[17] Such an asset of UV Raman is also anticipated to hold true for broad luminescence signals originating from precursor impurities during CVD-based synthesis or residual contamination associated with transfer processes of h-BN layers.[26,27]

Despite the advantages listed above, a potential drawback of UV Raman spectroscopy is that it may lead to the modification and/or strong degradation of the material under analysis, due to the high energy of the photons. Indeed, our present work demonstrates a destructive effect when employing UV excitation for Raman spectroscopy of thin h-BN films. The determinant impact is explicit in the gradual quenching of the h-BN's Raman signal during measurement and the local deformation of the surface, which coincides with the beam location. In some cases, long exposure time causes a complete disappearance of the Raman peak. Hence, the intuitive choice of long integration times during the measurement, aiming at the enhancement of the signal intensity, is not applicable and may potentially lead to a wrong interpretation of results regarding structural characteristics such as layer homogeneity and crystalline quality. At this point, the question arises: what is the reason for the strong signal degradation during UV Raman of h-BN, even though this material is expected to be thermally and chemically stable down to monolayer level? We hypothesize that this behavior is related to a combination of factors associated with the interaction of the UV laser with the h-BN, the ambient gas, and the substrate. In this contribution, we report on a systematic investigation aiming at the verification of these hypotheses. Time-decay Raman experiments in ambient pressure and vacuum were performed on h-BN films of different thicknesses grown by MBE on Ni templates and transferred to substrates offering different thermal stability. The aim of these experiments was twofold: (i) to study the type and degree of interaction of the UV laser excitation with each type of sample and ambient and (ii) to determine an optimized exposure time with minimum degradation of the Raman signal based on sample properties such as h-BN thickness and substrate type. The latter allows us to propose a straightforward solution for the use of UV Raman spectroscopy for the analysis of atomically thin h-BN films, including the use of a line-mapping methodology to enhance the signal-to-noise ratio (S/N ratio) of UV Raman spectra.

2 | EXPERIMENTAL

h-BN thin films were grown by MBE on Ni templates, which consisted of a 400-nm-thick Ni polycrystalline film on a sapphire substrate (Al_2O_3(0001)) with a size of 10 mm × 10 mm. For the synthesis of h-BN, a high-temperature effusion source is used to provide the boron beam, while a radio-frequency plasma source produces the active N species. The substrate was kept at 700°C during growth, and different growth times were utilized in order to prepare h-BN films with different thicknesses. More details about sample preparation can be found elsewhere.[17]

Transfer of the MBE-grown h-BN films is performed using a wet chemical transfer technique adapted from Suk et al.[28] First, the h-BN surface is spin coated with poly(methyl methacrylate) (PMMA) at 3000 rpm for 1 min, and then, the sample is immersed in a shallow beaker containing diluted nitric acid (10%) to etch the Ni film. After that, the floating PMMA/h-BN stack (about 9 mm × 9 mm) is rinsed in dilute HCl to remove residual Ni etchants as well as particles. Then, it is rinsed in deionized water and transferred onto 10 mm × 10 mm large substrates. Besides SiO_2 (100 nm thick, thermally grown on Si(100)), which is a standard substrate for transferred 2D materials, we also employed GaAs(001) and Al_2O_3(0001). Note that in order to allow for comparison, the h-BN films transferred to different types of substrates were grown simultaneously in the same growth experiment. This is followed by baking at 150°C on a hot plate to remove the water molecules trapped at the h-BN/substrate interface. As a last step, the PMMA coating is washed away in acetone. The average thickness of the transferred h-BN films, as well as their surface morphology, was obtained by depth profiling using atomic force microscopy (AFM) in tapping mode. In the present study, the transferred h-BN films possessed the following thicknesses: 2.5 ± 0.3 nm, 6.5 ± 0.2 nm, and 12.0 ± 2.5 nm. For the Raman spectroscopy studies, all measurements were conducted at room temperature either in air or vacuum (10^{-5} to 10^{-6} mbar) in a backscattering configuration using the intracavity frequency-doubled output of an Ar^+ ion laser at 244 nm for optical excitation. The laser light has been focused by an 80× objective to a spot of ~1 μm on the sample surface with a power of about 1 mW. This excitation power has been chosen for all measurements in order to obtain a S/N ratio, which allowed for proper spectral analysis of the samples investigated here. Even though the use of moderately reduced powers could partially mitigate the degradation of the samples (see Figures S1 and S2), the corresponding strong decrease of the S/N ratio for the h-BN Raman signal impeded time-decay Raman experiments at much lower laser power. The scattered light has been collected by the same objective, dispersed spectrally by an 80-cm Jobin-Yvon spectrograph (3600 lines/mm grating) and detected by a LN_2-cooled CCD camera. For line-scan measurements, a motorized sample stage has been utilized.

3 | RESULTS AND DISCUSSIONS

3.1 | Morphological characteristics

Figure 1 shows a collection of results which illustrates the morphological characteristics of the investigated samples. Figure 1a shows a photograph of an approximately 9 mm × 9 mm large h-BN film transferred to a SiO_2/Si substrate. In this case, the film is about 12.0 ± 2.5 nm thick and thus exhibits a very clear contrast to the underlying SiO_2. For thinner h-BN films and/or GaAs and Al_2O_3 substrates, a much weaker contrast is observed (not shown). Note that the square patterning seen at the central part of the SiO_2/Si substrate contains different types of nanopillar structures. Their effect on the Raman measurements will not be discussed here. In fact, all measurements displayed and discussed in the present study were performed outside such patterned areas. In Figure 1b–d, images taken for the 2.5 ± 0.3-nm-thick h-BN film are shown. Figure 1b illustrates an optical micrograph of an edge of this h-BN film after transfer to the SiO_2/Si substrate. One can see that the h-BN surface area is clean without the existence of large residual contamination originating, for instance, from PMMA. Moreover, the picture shows that the h-BN edge is defective with film tearing and folding taking place. Such areas were avoided for the Raman studies. Figure 1c depicts an AFM image of an edge for the same h-BN film. Corroborating Figure 1b, the AFM image shows that the film is continuous also within a microscopic scale. The film continuity and some thickness variation (i.e., the existence of brighter areas which correspond to regions where more h-BN layers formed) agree well with the AFM results obtained for the films before transfer (not shown). Examples of profile measurements, which were used to determine the average thickness of the transferred h-BN films, are presented in Figure 1d.

3.2 | Effect of continuous UV laser exposure on h-BN films

Figure 2a depicts Raman spectra collected under UV excitation under ambient conditions for the 12.0 ± 2.5-nm-thick h-BN film transferred onto SiO_2/Si. They serve to illustrate the degradation observed in the E_{2g} Raman peak of h-BN located around 1364 cm^{-1} as a function of

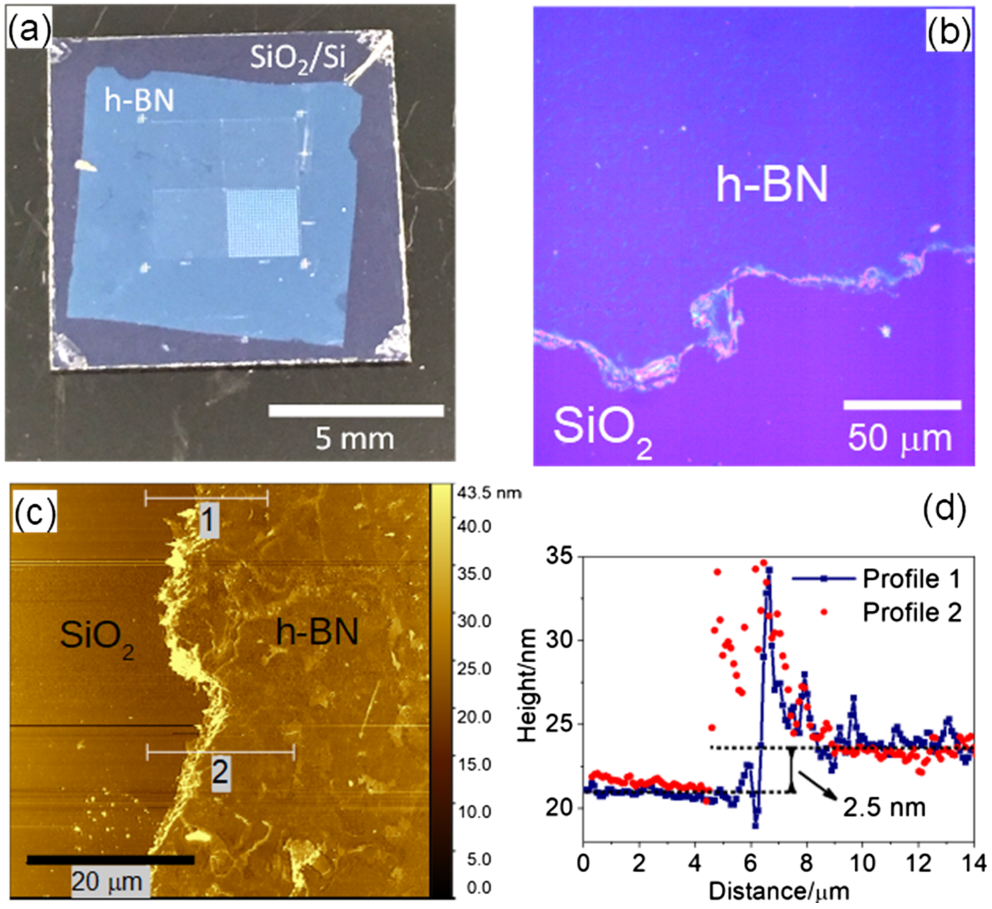

FIGURE 1 (a) Photograph of a sample containing a ~9 mm × 9 mm large hexagonal boron nitride (h-BN) film (thickness = 12.0 ± 2.5 nm) transferred to a SiO_2/Si substrate. (b) Optical micrograph showing the edge of a h-BN film (thickness = 2.5 ± 0.3 nm) transferred to SiO_2/Si. (c) Atomic force microscopy (AFM) image of an edge region of the same h-BN film. (d) Plots of the Profiles 1 and 2 depicted in white in (c). For them, a thickness of about 2.5 nm could be deduced for the transferred h-BN film. Note that the strong height oscillations correspond to the film edge region where defects such as layer tearing and folding are abundant, as visible in (b) and (c) [Colour figure can be viewed at wileyonlinelibrary.com]

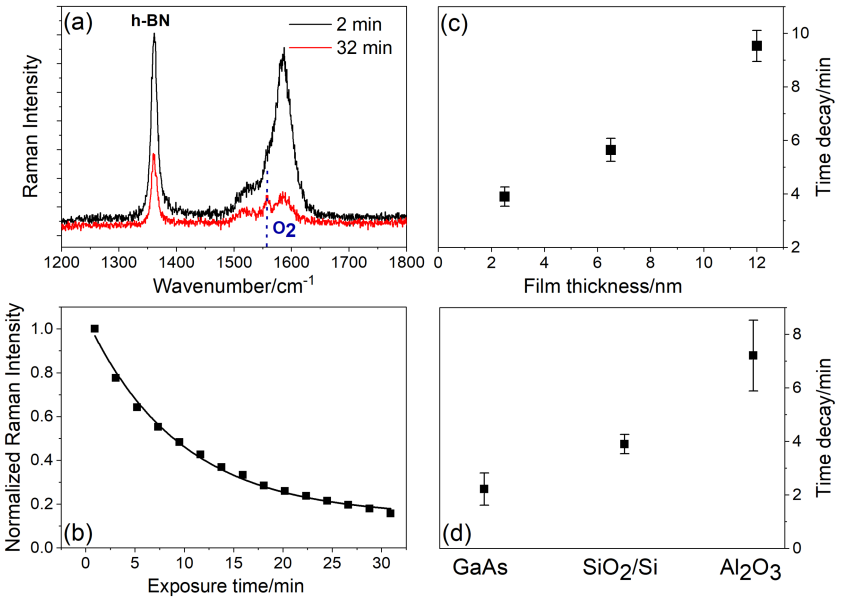

FIGURE 2 (a) UV Raman spectra for a 12.0 ± 2.5-nm-thick hexagonal boron nitride (h-BN) film transferred onto SiO_2/Si obtained after 2 and 32 min exposure times. (b) Normalized intensity of the E_{2g} Raman peak of h-BN as a function of exposure time for sequentially recorded spectra. The acquisition time for each individual spectrum was 2 min. The intensity axis was normalized with respect to the intensity of the first spectrum collected after 2 min of exposure (here plotted at half time of the total exposure time, i.e., 1 min). (c) Decay constant for the E_{2g} Raman mode of h-BN for films of different thicknesses transferred onto SiO_2/Si substrates. (d) Decay constant for the E_{2g} Raman mode of h-BN for 2.5 ± 0.3-nm-thick h-BN films transferred to GaAs, SiO_2/Si, and Al_2O_3 substrates [Colour figure can be viewed at wileyonlinelibrary.com]

time. For these experiments, the h-BN film was exposed continuously in the same surface spot while the Raman signal was collected after each 2 min. The spectra shown in Figure 2a correspond thus to the first and the last Raman signal measurement. It is clearly visible that the h-BN's peak intensity is strongly quenched as the exposure time to the UV laser excitation increases. Interestingly, the full width at half maximum (FWHM), which was determined by applying a peak fitting to the E_{2g} peak (Lorentzian function), does not significantly change for all measurements remaining at 11.8 ± 0.5 cm^{-1}. Note that this FWHM value is compared with what has been reported for state-of-the-art h-BN flakes and serves as an indication for the high crystalline

quality of our MBE-grown films.[13,17] Also, the position of the h-BN peak remains unaltered for all measurements. The peak at 1556 cm^{-1} corresponds to the vibrational mode of O_2 in the air,[17,29] while the broad band appearing between 1500 and 1600 cm^{-1} originates from a carbonaceous surface contamination, as it will be discussed later.

The evolution of the degradation in the Raman signal for all measurements is shown in Figure 2b, which is a plot of the normalized Raman area intensity as a function of UV exposure time. The observed time dependence is well described by an exponential decay

$$I_{SP}(t) = I_0 e^{-t/\tau}, \quad (1)$$

where τ is the characteristic decay constant. This finding suggests that degradation of the h-BN film inside the excitation spot takes place already during the acquisition of the first Raman spectrum.

The same kind of Raman intensity decay experiment was performed for the other samples containing transferred h-BN films with thicknesses of 2.5 ± 0.3 nm and 6.5 ± 0.2 nm. Similar to the thicker h-BN film, no significant changes in the FWHM and position of the Raman peaks were observed. The decay constant τ obtained by an exponential curve fitting of the data is plotted in Figure 2c as a function of the average film thickness. The faster decay obtained for reduced h-BN film thicknesses suggests that special attention must be given to UV Raman analysis of atomically thin h-BN films. As discussed earlier (see Figures S1 and S2), note that the use of a lower laser power (0.25 mW instead of 1 mW) could reduce degradation resulting thus in a slower decay of the signal (decay constant of 12 min instead of 3.9 min). One can anticipate that for h-BN surface coverages, which are only one to a few atomic layers thick, the use of integration times longer than 2 or 3 min using UV excitation (λ = 244 nm) may result in the complete quench of the Raman signal due to its temporal degradation. This, in turn, can lead to a wrong interpretation of the structural and morphological properties of the material.

At this point, it is important to address, even if from a qualitative viewpoint, the main effects associated with the degradation of the h-BN films under UV exposure. The first effect to be considered is the local heating of sample due to the interaction with the UV laser. Thermally activated chemical reactions may lead to a substitution or removal of the h-BN film, most likely around defective areas either created during growth (e.g., grain boundaries and point defects such as vacancies) or during transfer (e.g., cracks). In particular, oxidation of h-BN at elevated temperature might play a major role.[30,31] However, the fact that the width and position of the h-BN Raman peak remains unaltered during the time-decay experiments suggests that regions with oxidized h-BN (if not removed from the surface) do not contribute to E_{2g} mode. Due to the Gaussian intensity profile of the focused laser spot, one can speculate that the h-BN Raman signal originates mainly from the surface area excited by the outer ring of the laser spot, where either a reduced or no oxidation takes place given the lower heating in this region in comparison to the spot center. Finally, the increase of the decay constant for the E_{2g} h-BN signal as a function of the film thickness is probably related to the larger volume of available material and the accordingly improved heat dissipation.

The heating of the sample should occur due to the interaction of the UV laser not only with h-BN but also with the underlying substrate. Although the laser energy (5.08 eV) is smaller than the band gap of h-BN (around 6 eV),[1] a certain degree of absorption of UV light by the h-BN is expected, for instance, due to the existence of structural defects in the h-BN layers.[32] In fact, surface oxidation and even ablation induced by UV exposure have been reported for pulsed irradiation at a wavelength of 248 nm.[33,34] Moreover, considering now the substrate SiO_2/Si, while the high band gap of SiO_2 (8.9 eV)[35] makes it in principle transparent to the UV light, heating of the Si substrate (with an indirect band gap of 1.1 eV) located 100 nm below the SiO_2 surface should also contribute to heating during UV exposure.

Following the assumption that UV substrate heating plays a role in h-BN's heating and degradation, transferring the same type of h-BN films to other substrates offering optical band gap and thermal conductivity different from those of SiO_2/Si should lead to a systematical change in the stability of the h-BN film under UV exposure, that is, different decay constants τ should be observed. Hence, in addition to SiO_2/Si, we made use of GaAs(001) and Al_2O_3(0001) as transfer templates. While GaAs has a band gap of 1.4 eV,[36] Al_2O_3 is an ultra-wide band gap dielectric with reported values for the band gap ranging from 7 up to 8.8 eV.[35,37–39] Figure 2d depicts a comparison of the decay constants τ obtained by exponential curve fittings (see Figure S3) for the E_{2g} Raman intensity of 2.5 ± 0.3-nm-thick h-BN films transferred to GaAs, SiO_2/Si, and Al_2O_3 substrates. In comparison with SiO_2/Si, longer and shorter time-decay constants are, respectively, determined when Al_2O_3 and GaAs are employed. These results serve as an evidence for the contribution of the underlying material to the local heating and apparent degradation of the h-BN film. The sapphire substrate is transparent to the UV radiation due to its high energy band gap, meaning that its direct heating under the laser spot is a very inefficient if not an

inexistent process. Accordingly, the faster intensity decay observed for the other substrates is attributed to the strong optical absorption of UV light in GaAs and Si (absorption in SiO_2 with a band gap of about 9 eV can be neglected). The weaker decay for SiO_2/Si compared with GaAs substrates can be explained by the better heat dissipation. Whereas the optical absorption coefficient at 244 nm is smaller for Si by only 10% compared with GaAs,[40] the thermal conductivity in Si is three times larger than in GaAs.[41] In fact, a strong morphological change in the surface areas of the Raman measurements can be seen in the case of GaAs substrates. Figure 3 displays optical and AFM micrographs of such areas. It was observed by the objective of the Raman spectroscopy that the UV laser beam creates almost circular features just below the beam during the measurements. In Figure 3a, features created by several measurements performed following a line can be seen. From this image, it seems that the UV radiation creates holes on the surface of the sample. However, the AFM image in Figure 3b reveals that these features are actually large protrusions with heights reaching up to 2 μm. Although the reason for this behavior is not understood, it is possible that local melting of the GaAs leads to the creation of protrusions and thus to the full destruction of the uppermost h-BN film. The surface degradation upon UV exposure could be reduced by decreasing the laser power (see Figure S2). However, even after a power reduction by a factor of 20, it is still possible to identify surface damage.

In general, it is expected that the use of other excitation energies, which are higher than the direct band gap of the substrate material, will also result in heating of the substrate, which might contribute to the degradation of the h-BN Raman signal. Also, the optical absorption coefficients for many materials increase towards the UV spectral range, leading to particularly strong heating effects. Furthermore, the role of photochemistry might be more important in the UV spectral range.

3.3 | Suppression of chemical reactions: High-vacuum conditions

In order to verify whether or not chemical reactions with ambient gas molecules indeed play a major role in the decay of the UV Raman signal, we carried out experiments under high-vacuum conditions in an optical cryostat. Figure 4a displays Raman spectra of a 2.5-nm-thick h-BN film on a SiO_2/Si substrate measured after different exposure times. Besides the E_{2g} phonon peak from h-BN, all spectra exhibit the Si phonon line at 520 cm^{-1} from the substrate and the carbon-related peak at about 1600 cm^{-1}. The intensity of the E_{2g} phonon line again decreases with increasing exposure time (cf. Figure 2). At the same time, in striking difference to the case of ambient conditions, the carbon-related peak is found to increase. We attribute this peak to the formation of a carbonaceous adlayer at the h-BN surface, which likely originates from an UV-induced cracking of hydrocarbon molecules.[42] The temporal evolution of the different Raman signals is shown in Figure 4b. The decay constant of $\tau = 40$ min obtained for the h-BN signal constitutes an enhancement by one order of magnitude compared with ambient conditions (see Figure 2). This observation provides evidence for chemical reactions with ambient gas molecules being indeed the main reason for the decay of the Raman signal under UV exposure. The temporal evolution of the carbon-related peak indicates that the thickness of the carbonaceous adlayer on the h-BN surface grows during the UV exposure and finally reaches a saturation value. Indeed, the UV light-induced adsorption and desorption of ambient gas molecules depends

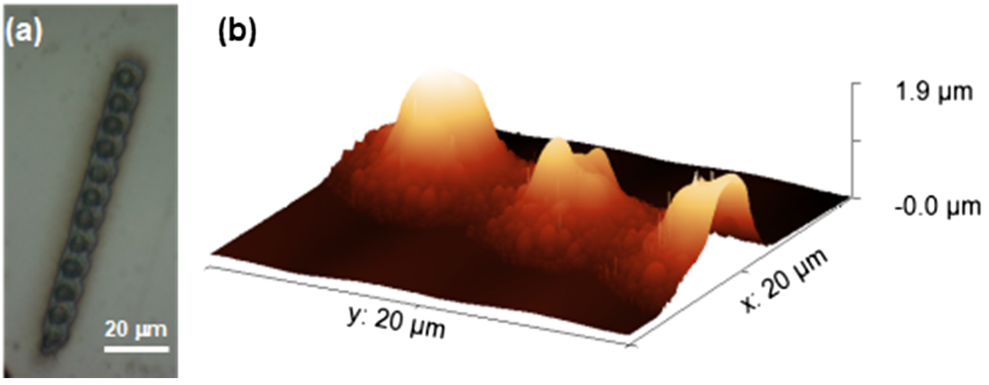

FIGURE 3 (a) Optical micrograph in differential interference contrast mode of a line of surface defects produced by UV laser exposure during Raman measurement of a ~2.5-nm-thick hexagonal boron nitride (h-BN) film transferred onto GaAs. The exposure time employed was 2 min. (b) Atomic force microscopy (AFM) image (in 3D representation) of some of the features shown in (a) [Colour figure can be viewed at wileyonlinelibrary.com]

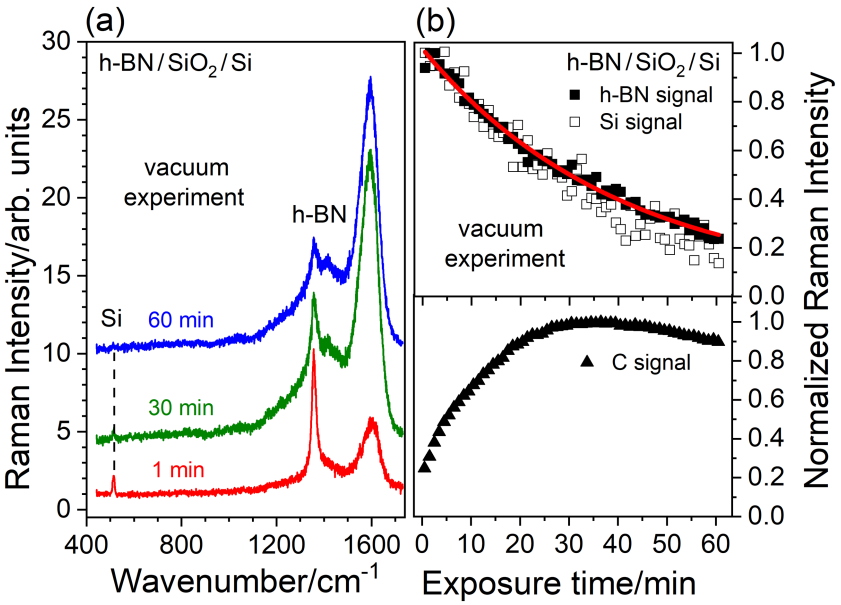

FIGURE 4 (a) UV Raman spectra for a 2.5-nm-thick hexagonal boron nitride (h-BN) film transferred onto SiO_2/Si obtained after different indicated exposure times. (b) Top: Normalized intensities of the E_{2g} peak from h-BN and the Si phonon line from the substrate as a function of exposure time. Bottom: Normalized intensity of the Raman peak around 1600 cm^{-1} from a carbonaceous surface contamination layer as a function of exposure time [Colour figure can be viewed at wileyonlinelibrary.com]

critically on the surface characteristics of the investigated sample, as shown previously for GaN and ZnO surfaces under ambient and vacuum conditions.[43–47] For the case of h-BN, it has been shown in Museur et al.[33] that UV irradiation leads to the formation of nitrogen vacancies and the breaking of B–N bonds, which promotes oxidation processes at the h-BN surface. The suppressed oxidation under vacuum conditions leads to qualitatively different surface characteristics,[33] which might be favorable for the formation of a carbonaceous adlayer and, thus, cause the observed temporal evolution of the carbon-related Raman intensity in our spectra. In fact, h-BN films are considered to be promising regarding their application as templates for organic adsorbates.[48–50]

Remarkably, the time dependence of the Si Raman signal from the substrate resembles closely that of the h-BN peak, as shown in Figure 4b. This finding strongly suggests a common origin for both decays. Consequently, we attribute this coincidence to the optical absorption of the incoming and backscattered UV light in the carbonaceous adlayer. Accordingly, the saturation of the carbon-related signal is explained partly by the optical probing in the carbonaceous adlayer, which is limited by optical absorption. Altogether, the measurements under vacuum reveal that the remaining slow decay of the h-BN Raman signal is mostly due to the formation of a carbonaceous adlayer with chemical reactions at the h-BN surface almost completely suppressed. In order to further reduce the decay of the h-BN Raman signal, an ozone cleaning in the optical cryostat as described in Brandt et al.[51] could be utilized. However, it has to be taken into account that this type of treatment can also potentially result into structural changes in the h-BN, such as defect formation and oxidation.[52,53]

3.4 | Approach for improvement of S/N ratio: Line-scan method

The S/N ratio in Raman spectra is known to increase with the total integrated signal I_{tot} accumulated during the acquisition time T because the photon shot noise is proportional to the square root of I_{tot}.[54] In the case of single spot measurements with $T > \tau$, we obtain for the UV Raman spectra from h-BN films (cf. Equation 1):

$$I_{tot}^{sp} = I_0 \int_0^T e^{-t/\tau} dt = \tau \left(1 - e^{-T/\tau}\right) I_0. \quad (2)$$

Accordingly, the total signal I_{tot} saturates for long integration times ($T >> \tau$) at τI_0, which defines a limit for the S/N ratio. Furthermore, the time-averaged signal $(\tau/T)I_0$ decreases with increasing acquisition time (T) and is, therefore, not a measure for the initial signal strength I_0. However, the knowledge of the decay constants for different substrates and h-BN film thicknesses from the above Raman signal decay measurements (see Figure 2) enables the choice of an appropriate acquisition time ($T \approx \tau$) for single spot measurements.

In order to circumvent the disadvantages of single spot measurements under ambient conditions, we introduce an approach for the improvement of the S/N ratio in UV Raman spectra recorded under ambient conditions. We avoid the saturation of the integrated Raman signal by recording N spectra along a line with a separation larger than the laser-focus size between the single spot measurements. Accordingly, each individual acquisition is initiated at a spot which has not been exposed to UV light before. Choosing an acquisition time of $\Delta T = \eta\tau$ for the individual spectra, the

total integrated Raman signal accumulated during the total time $T = N\Delta T$ corresponds to the sum of the individual spectra given by

$$I_{\text{tot}}^{ls} = NI_0 \int_0^{\Delta T} e^{-t/\tau} dt = N\tau\left(1 - e^{-\Delta T/\tau}\right) I_0 = T\eta^{-1}(1 - e^{-\eta}) I_0. \quad (3)$$

For the proposed line-scan method, the integrated signal is proportional to the acquisition time T without any saturation effect for the S/N ratio. The time-averaged signal is given by $\eta^{-1}(1 - e^{-\eta})I_0$ independent of the acquisition time T. Regarding the lower limit of $\Delta T(\eta)$, the detector dark current and read noise have to be taken into account which do not depend on the signal level I_{tot}.[54]

The advantage of the line-scan method is illustrated in Figure 5 by the comparison with a single spot measurement for a 2.5-nm-thick h-BN film on $Al_2O_3(0001)$. The line scan result corresponds to the average signal of 10 spectra recorded with a spatial separation of 2 μm. The spectrum for the single spot measurement, as well as each spectrum of the line scan, was recorded with the same exposure time. Indeed, the S/N ratio for the detection of the h-BN Raman signal is clearly improved for the line-scan spectrum. Using an exposure time for a single spot measurement similar to the total time employed for the line scan would lead to a strong degradation or quenching of the Raman signal. Note that layer inhomogeneities (e.g., strain and thickness variation) at a micrometer scale might pose a limit for the line-scan method due to broadening and shift of the Raman peak. However, for cases where the Raman signal is strong enough, one can in principle address such kind of inhomogeneities by the analysis of individual line-scan spectra and a variation of the spatial line-scan length.

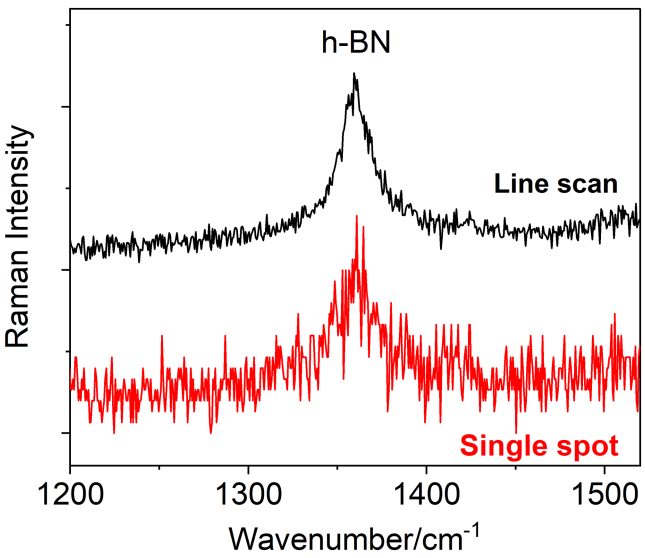

FIGURE 5 UV Raman spectra obtained for a ~2.5-nm-thick hexagonal boron nitride (h-BN) film transferred onto $Al_2O_3(0001)$. A comparison between a single spot measurement and the averaging of a line scan composed of 10 measurements is made. The spectra are shifted in the vertical axis for better visualization [Colour figure can be viewed at wileyonlinelibrary.com]

4 | CONCLUSIONS

The excitation of Raman spectra with UV light (244 nm) under ambient conditions results in a temporal decay of the signal from h-BN films. The decrease of the Raman intensity is caused by thermally activated reactions of the h-BN surface with ambient gas molecules. Under vacuum conditions, the chemical reactions are suppressed, but the h-BN surface is progressively contaminated with a carbonaceous adlayer. The S/N ratio under ambient conditions can be strongly improved by line-scan measurements.

ACKNOWLEDGEMENTS

Marwa Karim acknowledges the German Academic Exchange Service (Deutscher Akademischer Austaushdienst [DAAD]) and the Ministry of Higher Education and Scientific Researches (MHESR) in Egypt. A postdoctoral scholarship was awarded to her under the German Egyptian Research Short-Term Programme (GERSS), 2018–2019 (Program ID: 57397533). The authors acknowledge H.P. Schönherr, C. Herrmann, C. Stemmler, C. Morgenroth, and W. Seidel for their technical support. Moreover, Michael Hanke is acknowledged for the critical reading of the manuscript. Open access funding enabled and organized by Projekt DEAL.

ORCID

Joao Marcelo J. Lopes https://orcid.org/0000-0001-5268-1862

REFERENCES

[1] J. D. Caldwell, I. Aharonovich, G. Cassabois, J. H. Edgar, B. Gil, D. N. Basov, *Nat. Rev. Mater.* **2019**, *4*, 553.
[2] A. Maity, S. J. Grenadier, J. Li, J. Y. Lin, H. X. Jiang, *J. Appl. Phys.* **2018**, *123*, 044501.
[3] C. R. Dean, A. F. Young, I. Meric, C. Lee, L. Wang, S. Sorgenfrei, K. Watanabe, T. Taniguchi, P. Kim, K. L. Shepard, J. Hone, *Nat. Nanotechnol.* **2010**, *5*, 722.
[4] F. Cadiz, E. Courtade, C. Robert, G. Wang, Y. Shen, H. Cai, T. Taniguchi, K. Watanabe, H. Carrere, D. Lagarde, M. Manca, T. Amand, P. Renucci, S. Tongay, X. Marie, B. Urbaszek, *Phys. Rev. X* **2017**, *7*, 021026.

[5] E. Courtade, B. Han, S. Nakhaie, C. Robert, X. Marie, P. Renucci, T. Taniguchi, K. Watanabe, L. Geelhaar, J. M. J. Lopes, B. Urbaszek, *Appl. Phys. Lett.* **2018**, *113*, 032106.
[6] R. T. Paine, C. K. Narula, *Chem. Rev.* **1990**, *90*, 73.
[7] L. H. Li, J. Cervenka, K. Watanabe, T. Taniguchi, Y. Chen, *ACS Nano* **2014**, *8*, 1457.
[8] Z. Liu, Y. Gong, W. Zhou, L. Ma, J. Yu, J. C. Idrobo, J. Jung, A. H. MacDonald, R. Vajtai, J. Lou, P. M. Ajayan, *Nat. Commun.* **2013**, *4*, 2541.
[9] A. Laturia, M. L. Van de Put, W. G. Vandenberghe, *NP 2D Mater. Appl.* **2018**, *2*, 6.
[10] H. Tian, Y. He, P. Das, Z. Cui, W. Shi, A. Khanaki, R. K. Lake, J. Liu, *Adv. Mater. Interfaces* **2019**, *6*, 1901198.
[11] A. Hernández-Mínguez, J. Lähnemann, S. Nakhaie, J. M. J. Lopes, P. V. Santos, *Phys. Rev. Appl.* **2018**, *10*, 044031.
[12] S. J. Haigh, A. Gholinia, R. Jalil, S. Romani, L. Britnell, D. C. Elias, K. S. Novoselov, L. A. Ponomarenko, A. K. Geim, R. Gorbachev, *Nat. Mater.* **2012**, *11*, 764.
[13] R. V. Gorbachev, I. Riaz, R. R. Nair, R. Jalil, L. Britnell, B. D. Belle, E. W. Hill, K. S. Novoselov, K. Watanabe, T. Taniguchi, A. K. Geim, P. Blake, *Small* **2011**, *7*, 465.
[14] S. A-Rang Jang, C. Hong, S. I. Hyun, G. Yoon, H. Y. Kim, T. J. Jeong, S. O. Shin, K. Park, S. K. Wong, N. Kwak, K. Y. Park, E. Choi, A. Mishchenko, F. Withers, K. S. Novoselov, H. Lim, H. S. Shin, *Nano Lett.* **2016**, *16*, 3360.
[15] X. Li, S. Sundaram, Y. E. Gmili, T. Ayari, R. Puybaret, G. Patriarche, P. L. Voss, J. P. Salvestrini, A. Ougazzaden, *Cryst. Grow. Des.* **2016**, *16*, 3409.
[16] M. Sky Driver, J. D. Beatty, O. Olanipekun, K. Reid, A. Rath, P. M. Voyles, J. A. Kelber, *Langmuir* **2016**, *32*, 2601.
[17] S. Nakhaie, M. Heilmann, T. Krause, M. Hanke, J. M. J. Lopes, *J. Appl. Phys.* **2019**, *125*, 115301.
[18] M. Heilmann, A. S. Prikhodko, M. Hanke, A. Sabelfeld, N. I. Borgardt, J. M. J. Lopes, *ACS Appl. Mater. Interfaces* **2020**, *12*, 8897.
[19] D. J. Pennachio, C. C. Ornelas-Skarin, N. S. Wilson, S. G. Rosenberg, K. M. Daniels, R. L. Myers-Ward, D. K. Gaskill, C. R. Eddy Jr., C. J. Palmstrøm, *J. Vac. Sci. Technol. A* **2019**, *37*, 051503.
[20] Y.-J. Cho, A. Summerfield, A. Davies, T. S. Cheng, E. F. Smith, C. J. Mellor, A. N. Khlobystov, C. T. Foxon, L. Eaves, P. H. Beton, S. V. Novikov, *Sci. Rep.* **2016**, *6*, 34474.
[21] J. M. Wofford, S. Nakhaie, T. Krause, X. Liu, M. Ramsteiner, M. Hanke, H. Riechert, J. M. J. Lopes, *Sci. Rep.* **2017**, *7*, 43644.
[22] A. C. Ferrari, J. C. Meyer, V. Scardaci, C. Casiraghi, M. Lazzeri, F. Mauri, S. Piscanec, D. Jiang, K. S. Novoselov, S. Roth, A. K. Geim, *Phys. Rev. Lett.* **2006**, *97*, 187401.
[23] F. Fromm, M. H. Oliveira Jr., A. Molina-Sanchez, M. Hundhausen, J. M. J. Lopes, H. Riechert, L. Wirtz, T. Seyller, *New J. Phys.* **2013**, *15*, 043031.
[24] S. Reich, A. C. Ferrari, R. Arenal, A. Loiseau, I. Bello, J. Robertson, *Phys. Rev. B* **2005**, *71*, 205201.
[25] I. Pócsik, M. Hundhausen, M. Koós, L. Ley, *J. Non Cryst. Solids* **1998**, *227*, 1083.
[26] Z. Liu, L. Song, S. Zhao, J. Huang, L. Ma, J. Zhang, J. Lou, P. M. Ajayan, *Nano Lett.* **2011**, *11*, 2032.
[27] A. G. F. Garcia, M. Neumann, F. Amet, J. R. Williams, K. Watanabe, T. Taniguchi, D. Goldhaber-Gordon, *Nano Lett.* **2012**, *12*, 4449.
[28] J. W. Suk, A. Kitt, C. W. Magnuson, Y. Hao, S. Ahmed, J. An, A. K. Swan, B. B. Goldberg, R. S. Ruoff, *ACS Nano* **2011**, *5*, 6916.
[29] A. Weber, E. A. McGinnis, *J. Mol. Spectrosc.* **1960**, *4*, 195.
[30] V. A. Lavrenko, A. F. Alexeev, *Ceram. Int.* **1986**, *12*, 25.
[31] K. Oda, T. Yoshio, *J. Mater. Sci.* **1993**, *28*, 6562.
[32] T. Q. P. Vuong, G. Cassabois, P. Valvin, E. Rousseau, A. Summerfield, C. J. Mellor, Y. Cho, T. S. Cheng, J. D. Albar, L. Eaves, C. T. Foxon, P. H. Beton, S. V. Novikov, B. Gil, *2D Mater.* **2017**, *4*, 021023.
[33] L. Museur, D. Anglos, J.-P. Petitet, J.-P. Michel, A. V. Kanaev, *JOL* **2007**, *127*, 595.
[34] V. V. Kononenko, M. S. Komlenok, M. A. Dezhkina, V. M. Gololobov, V. I. Konov, *Quantum Electron.* **2018**, *48*, 996.
[35] D. G. Schlom, S. Guha, S. Data, *MRS Bull.* **2008**, *33*, 1017.
[36] J. S. Blakemore, *J. Appl. Phys.* **1982**, *53*, R123.
[37] S. D. Singh, M. Nand, A. Das, R. S. Ajimsha, A. Upadhyay, R. Kamparath, D. K. Shukla, C. Mukherjee, P. Misra, S. K. Rai, A. K. Sinha, S. N. Jha, D. M. Phase, T. Ganguli, *J. Appl. Phys.* **2016**, *119*, 165302.
[38] F. Zhang, K. Saito, T. Tanaka, M. Nishio, M. Arita, Q. Guo, *Appl. Phys. Lett.* **2014**, *105*, 162107.
[39] J. Y. Tsao, S. Chowdhury, M. A. Hollis, D. Jena, N. M. Johnson, K. A. Jones, R. J. Kaplar, S. Rajan, C. G. Van de Walle, E. Bellotti, C. L. Chua, R. Collazo, M. E. Coltrin, J. A. Cooper, K. R. Evans, S. Graham, T. A. Grotjohn, E. R. Heller, M. Higashiwaki, M. S. Islam, P. W. Juodawlkis, M. A. Khan, A. D. Koehler, J. H. Leach, U. K. Mishra, R. J. Nemanich, R. C. N. Pilawa-Podgurski, J. B. Shealy, Z. Sitar, M. J. Tadjer, A. F. Witulski, M. Wraback, J. A. Simmons, *Adv. Elec. Mater.* **2017**, *4*, 1600501.
[40] D. E. Aspnes, A. A. Studna, *Phys. Rev. B* **1983**, *27*, 985.
[41] P. D. Maycock, *Solid-State Electron.* **1967**, *10*, 161.
[42] H. D. Wanzenboeck, P. Roediger, G. Hochleitner, E. Bertagnolli, W. Buehler, *J. Vac. Sci. Technol. A* **2010**, *28*, 1413.
[43] C. Netzel, J. Jeschke, F. Brunner, A. Knauer, M. Weyers, *J. Appl. Phys.* **2016**, *120*, 095307.
[44] M. Foussekis, A. A. Baski, M. A. Reshchikov, *Appl. Phys. Lett.* **2009**, *94*, 162116.
[45] M. Z. Iqbal, M. A. Reshchikov, L. He, H. Morkoç, *J. Electron. Mater.* **2003**, *32*, 346.
[46] J. A. Röhr, J. Sá, S. J. Konezny, *Commun. Chem.* **2019**, *2*, 52.
[47] J. Bao, I. Shalish, Z. Su, R. Gurwitz, F. Capasso, X. Wang, Z. Ren, *Nanoscale Res. Lett.* **2011**, *6*, 404.
[48] W. Auwärter, *Surf. Sci. Rep.* **2019**, *74*, 1.
[49] H. Kobayashi, A. Fukuoka, *J. Phys. Chem. C* **2017**, *121*, 17332.
[50] M. I. Baraton, T. Merle, P. Quintard, V. Lorenzelli, *Langmuir* **1993**, *9*, 1486.
[51] O. Brandt, T. Flissikowski, D. M. Schaadt, U. Jahn, A. Trampert, H. T. Grahn, *Appl. Phys. Lett.* **2008**, *93*, 081907.
[52] S. J. Cartamil-Bueno, M. Cavalieri, R. Wang, S. Houri, S. Hofmann, H. S. J. van der Zant, *NPJ 2D Mater. Appl.* **2017**, *1*, 16.

[53] S. W. King, R. J. Nemanich, R. F. Davis, *Surf. Interface Anal.* **2015**, *47*, 798.
[54] M. Konnik, *J. Welsh, arXiv* **2014**, *1412*, 4031.

SUPPORTING INFORMATION

Additional supporting information may be found online in the Supporting Information section at the end of this article.

How to cite this article: Karim M, J. Lopes JM, Ramsteiner M. The impact of ultraviolet laser excitation during Raman spectroscopy of hexagonal boron nitride thin films. *J Raman Spectrosc*. 2020;51:2468–2477. https://doi.org/10.1002/jrs.6007